Look-alike Landau levels in locally biased twisted bilayer graphene

Tomasz Chwiej*
AGH University of Science and Technology, al. A. Mickiewicza 30, 30-059 Cracow, Poland

The large lattice constant of Moire superlattice formed in twisted bilayer graphene for small twist enables observing the Landau levels splitting into Hofstadter butterflies in energy spectra for moderate magnetic field. This is expected for generic system under homogeneous bias conditions but its robustness against spatial potential fluctuations is left open question. We study the energy structure of twisted bilayer system in dependence of both, the homogeneous magnetic field and the bias voltage applied exclusively in its central part. Although the translational symmetry is broken, the energy states mainly localized outside the central region may still condense on Landau levels and these would split revealing self-similarity feature. Moreover, besides the generic branch of energy states with zero-mode Landau level at charge neutrality point, when both layers are biased with the same voltage, the second look-alike energy branch shifted upwards can be developed by states largely localized in central region. Otherwise, for counter-biasing of layers, only generic branch exists but with lowest Landau layers flanked by either, hole-like and electron-like states localized at the top or at the bottom layer of central biased part of twisted bilayer system.

I. INTRODUCTION

Twisted bilayer graphene belong to class of layered van der Waals materials[1] and it is prepared by placing one graphene layer onto another, by means of CVD, pick-up or MBE techniques,[2–6] that the crystallographic axes in both layers differ by small twist angle θ. Honeycomb graphene lattice is composed of two interpenetrating triangle A and B sublattices of carbon atoms and these, due to the twist angle, periodically move closer to and away from their counterparts in second layer leading to formation of Moire lattice. That introduces new length scale $L_m = a_0/2/\sin(\theta/2)$ ($a_0 = 0.246$ nm is graphene lattice constant) defining thus spatial periodicity of interlayer, or more precisely, AA and AB/BA intersublattice couplings. Consequently, the energy structure is renormalized developing Moire bands irrespective commensurability of Moire lattice occurs or not.[7–11] As show theoretical and experimental works, strong local interlayer coupling makes the particles wave functions to be largely localized at AA sites[12–15] especially for the set of magic twist angles when Fermi velocity is strongly suppressed due to flattening of low energy bands.[9–11,16] Spatial localization of Dirac particles may be further enhanced in TBLG for small twist angles $\theta << 1^0$ when atomic lattice reconstruction in both layers spontaneously occurs[4] forming topologically protected one-dimensional transport channels along the edge of adjacent AB and BA triangles,[6,17] the regions of strong pseudomagnetic field.[18] Flattening of low energy bands decreases their bandwidths making single particle kinetic energy comparable with electron-electron interactions in TBLG. That gives rise to spectacular correlations effects observed experimentally in recent years such as unconventional superconductivity,[19,20] correlated insulating phases,[21,22] large orbital magnetism[2,23,24] and anomalous Hall ferromagnetism.[25,26]

Since TBLG enables engineering single particle properties, what results directly from dependence of Moire energy bands on twist angle, its remarkable features can be fine tuned giving rise to twisttronics.[27] Possibility of changing the Moire lattice constant in wide range allows to observe experimentally the Hofstadter butterflies.[28] The fractal pattern in energy spectrum of TBLG is evoked for moderate magnetic fields when the magnetic flux $\phi_M = BS_M$ for single Moire cell extending over few tens of nanometers is of the same order as magnetic flux quantum ϕ_0, unattainable condition for conventional atomic lattices. Theoretical works of Bistritzer and MacDonald[29] for infinite TBLG as well as of Wang et al.[30] for spatially limited TBLG system predicted Landau levels splitting to form fractal pattern for magnetic field range depending explicitly on twist angle. This effect was later observed experimentally.[5,31]

In present work we analyze formation of Landau levels in TBLG electrostatically biased in its center. Our considerations correspond to strongly coupled twisted bilayer system that is formed for low twist $\theta = 0.75^0 - 2^0$. It is known that the variations of barrier's height combined with various energies of incident electron in TBLG may induce not only oscillations in transmission through the barrier but even lead to its complete suppressing.[32] Thus, the combined effect of electrostatic and magnetic deflection imposed on trajectory of Dirac particle shall substantially influence on Landau levels energy spectra. Our results show doubling of the number of states in energy spectra. The second look-alike Landau levels energy branch is shifted by about of bias voltage applied to layers provided that polarization of both layers is identical. Otherwise, when layers are counter-biased, doubling of energy states does not occur. Instead, we observe two flanking states detached from the lowest Landau levels, these have electron-like or hole-like nature. Contrary to ordinary Landau levels, these states are localized within biased region and therefore their energies linearly depend on amplitude of applied voltage. For identical biasing of layers there is only one flanking state with constant slope depending on a sign of the bias voltage $\partial E/\partial V_{bias} \sim sign(V_{bias})$.

The paper is organized in the following way, in Sec.II

we briefly describe the theoretical model and applied numerical method, results are presented Sec.III along with discussion, conclusions are given in Sec.IV.

II. THEORETICAL MODEL

We consider finite size TBLG system within circular region for $r \leq r_{max} = 150$ nm. The potential bias is applied in its center with formula

$$V_\alpha(r) = \frac{V_\alpha}{1+\exp\left(\frac{r-R_c}{\sigma}\right)}, \tag{1}$$

and defines the electrostatic cavity of radius $R_c = 80$ nm with respect to rest part of TBLG system, $\alpha = t, b$ labels top and bottom layer, respectively. Two cases are analyzed in detail, first, an identical bias potential is applied to layers $V_t = V_b$ while in second case these are counterpolarized $V_t = -V_b$. The edge of cavity is smooth and its effective width $2\sigma = 10$ nm is comparable with Moire length scale L_m considered in work. That ensures optimal conditions for trajectory deflection[32] and separation of states largely localized in cetral region from the outer ones. To mimic open boundaries for $r > r_{out}$ and to minimize its influence on electronic states localized in central part we add complex absorbing potential[33–35] (V_{cap}) near the boundary $r > r_{cap} = 130$ nm

$$V_{cap}(r) = i\,\ln^2\left(1-\frac{r-r_{cap}}{r_{max}-r_{cap}}\right) \tag{2}$$

where $i = \sqrt{-1}$. Large dimensions of considered TBLG system guarantees minimal influence of edge states on electronic spectrum.[36] Our main aim is to show how the Landau levels are formed in TBLG when both graphene layers are locally biased. In calculations we use the continuum model of TBLG which gives reasonable results for low energy states. The advantage of this method results from the fact that it allows us to simulate TBLG systems of larger dimensions than e.g. tight-binding method. On the other hand, continuum model requires much attention paid to spatial symmetries that has to be taken into account which issue is largely avoid when atomistic calculations are made. Here we use TBLG Hamiltonian proposed by Bistritzer and MacDonald[9]

$$\hat{H}_{TBLG} = \begin{bmatrix} \hat{H}_t(-\theta/2) & \hat{W} \\ \hat{W}^\dagger & \hat{H}_b(\theta/2) \end{bmatrix} \tag{3}$$

where $\hat{H}_{t/b}$ is single layer Hamiltonian

$$\hat{H}_\alpha(\pm\theta/2) = \begin{bmatrix} U_\alpha & v_F e^{\pm i\theta/2}\hat{\Pi}^\dagger \\ v_F e^{\mp i\theta/2}\hat{\Pi} & U_\alpha \end{bmatrix} \tag{4}$$

twisted by $\pm\theta/2$ with respect to x axis, $U_\alpha = V_\alpha + V_{cap}$, $v_F \approx 10^6$ m/s is Fermi velocity in graphene and $\hat{\Pi} = \hat{\pi}_x + i\hat{\pi}_y$, $\hat{\boldsymbol{\pi}} = \hat{\boldsymbol{p}} + e\boldsymbol{A}$ where $\hat{\boldsymbol{p}}$ is momentum operator. The vector potential is taken in symmetric form $\boldsymbol{A} = B[-y, x, 0]$ which leaves rotational symmetry of $\hat{H}_\alpha(\pm\theta/2)$ unchanged. The intersublattice coupling matrix elements are defined using identity matrix σ_0 and Pauli matrices $\sigma_x, \sigma_y, \sigma_z$ as $W = w_0\sum_{j=1}^{3}\tau_j e^{i\boldsymbol{Q}_j\boldsymbol{r}}$ where $\tau_1 = \sigma_0 + \sigma_x$, $\tau_2 = e^{i3\pi/2}e^{i\pi/3\sigma_z}\tau_1 e^{-i\pi/3\sigma_z}$ and $\tau_3 = \tau_2^*$. The reciprocal lattice vectors are defined as $\boldsymbol{Q}_j = K_\theta[\sin(\alpha_j), \cos(\alpha_j)]$ for $\alpha_j = \pi/2 + (j-1)2\pi/3$, $K_\theta = 8\pi\sin(\theta/2)/(3a_0)$ and $\boldsymbol{r} = r[\sin(\varphi), \cos(\varphi)]$ is position vector. The plane waves are expanded into a series of the Bessel function of first kind

$$e^{i\boldsymbol{Q}_j\boldsymbol{r}} = \sum_{n=-\infty}^{\infty} i^n J_n(Q_j r)e^{in(\varphi-\alpha_j)}. \tag{5}$$

This expansion in conjunction with explicit form of intersublattice hopping matrices τ_i gives the intersublattice coupling elements $w_{\mu\nu}$ (μ, $\nu = \{A, B\}$)

$$w_{\mu\nu} = 3w_0\sum_{k=-\infty}^{\infty} J_{3k+\eta}(Qr)e^{i(3k+\eta)\varphi} \tag{6}$$

where $\eta = +1, 0, -1$ for $w_{AA} = w_{BB}$, w_{AB} and w_{BA}, respectively. The strength of interlayer coupling is scaled by $w_0 = 110$ meV, however in unpatterned TBLG due to surface corrugation its value can be smaller for AA sites than for Bernal stacking regions.[37] Eigenvectors of TBLG Hamiltonian given in Eq.3 are four-component spinors $\Psi(\boldsymbol{r}) = [\psi_{A_t}(\boldsymbol{r}), \psi_{B_t}(\boldsymbol{r}), \psi_{A_b}(\boldsymbol{r}), \psi_{B_b}(\boldsymbol{r})]^T$. We use finite element method to solve this eigenvalue problem. The interlayer coupling potentials expressed in Eq.6 explicitly depends on set of angular momenta ($l = 3k + \eta$) and keeping in mind that single layer Hamiltonians have rotational symmetry it is reasonable to project the problem onto cylindrical coordinates. Then components of the four-spinor can be expressed in a basis of products of radial $\{f_m(r)\}$ and angular momentum states $\{e^{il\varphi}\}$

$$\psi_\lambda(r, \varphi) = \sum_{m, l_\lambda} c_{\lambda, m, l_\lambda} f_m(r)e^{il_\lambda\varphi} \tag{7}$$

where $\lambda \in \{A_t, B_t, A_b, B_b\}$ labels particular sublattice, m enumerates the radial elements taken as Hermite polynomials, l_λ is the angular momentum and c_{λ,m,l_λ} are linear expansion coefficients. With the above form of wave function the matrix elements of coupling potential take simple real-value form

$$\begin{aligned}&\langle f_{m_\mu}e^{il_\mu\varphi}|w_{\mu\nu}|f_{m_\nu}e^{il_\nu\varphi}\rangle = \\ &6\pi(-1)^{\max(0,\,l_\mu-l_\nu)}\,\delta_{l_\mu-l_\nu,3k+\eta} \\ &\times\int_0^{r_{max}} dr\, r\, f_{m_\mu}(r)\, f_{m_\nu}(r)\, J_{|l_\mu-l_\nu|}(Qr)\end{aligned} \tag{8}$$

where r_{max} is the radius of system, $\delta_{l_\mu - l_\nu, 3k+\eta}$ is Kronecker's delta which matches the angular momentum of both, the upper and the lower layer's states, with infinite series defining the coupling potential (Eq.6). Owing to this fact, the non-zero elements generally constitute an infinite sequence for $l_\mu - l_\nu = 3k + \eta, \quad k = 0, \pm 1, \pm 2, \ldots$. Actually for finite r_{max} this sequence also becomes finite because the Bessel function $J_{|l_\mu - l_\nu|}$ in the integral (Eq.8) quickly tends to zero for increasing angular momentum difference $|l_\mu - l_\nu|$. Finally the eigenvalue problem takes generalized form $\boldsymbol{H}\Psi = E\boldsymbol{S}\Psi$ which was effectively solved by exploiting sparsity of Hamiltonian and overlap integrals matrices. In calculations the radial elements have equal width $\Delta r = 2$ nm giving 75 elements while the maximal angular momentum that gives rise to energy is limited to $|l_\lambda| \leq 360$. Artificial absorbing potential (V_{cap}) included in our model, on one hand allows to mimic the nanostructure of infinite dimensions, but on the other hand it destroys the hermiticity of TBLG Hamiltonian. The imaginary part of eigenenergy ($E_\alpha = \varepsilon_\alpha - i\gamma_\alpha$) determines the coupling strength between the α state and the continuum part of energy spectra, its small value means weak coupling and vice versa.

Diagonalization provides us with two sets of the right and the left wave vectors $\{\Psi_i^{(r/l)}\}$ which are four-spinors $\Psi_i^{(r/l)} = \sum_\mu \psi_{i,\mu}^{(r/l)} \boldsymbol{e}_\mu$ and $\boldsymbol{e}_\mu$ are the 4-dimensional Cartesian basis vectors. These we use to approximate the retarted Green function in this space $G^R(E) = \sum_{\mu,\nu} G^R_{\mu,\nu}(E) \boldsymbol{e}_\mu \otimes \boldsymbol{e}_\nu$ with matrix elements $G^R_{\mu\nu}(E) = \sum_i \psi^r_{i,\mu} (\psi^l_{i,\nu})^* / (E - E_i)$. Having G^R we calculate the matrix elements of spectral function $\rho_{\mu\nu}(\boldsymbol{r}, \boldsymbol{r'}, E) = (i/2\pi)[G^R - (G^R)^\dagger]_{\mu\nu}$, density of states (DOS) $D(E) = Tr\{\rho(\boldsymbol{r}, \boldsymbol{r'}, E)\}$, local density of states (LDOS) $\rho(\boldsymbol{r}, E) = \sum_\mu \rho_{\mu\mu}(\boldsymbol{r}, \boldsymbol{r}, E)$ and, x and y components of magnetic current ($\boldsymbol{j} = dH/d\boldsymbol{A}$) $\boldsymbol{j}(\boldsymbol{r}, E) = -qv_F \sum_{\mu,\nu} \rho_{\mu,\nu}(\boldsymbol{r}, \boldsymbol{r}, E) \boldsymbol{e}_\nu^T (\tau_0 \otimes \boldsymbol{\sigma}) \boldsymbol{e}_\mu$. These quantities are defined for given energy E which in e.g. scanning tunneling spectroscopy (STS) is not well defined due thermal smearing, for this reason we average considered quantity O over energy for temperature $T = 4.2$ K as an integral $\langle O \rangle = \int dE'\, w(E', E, T)\, O(E')$ with window function taken as derivative of Fermi-Dirac distribution function $w(E', E, T) = -df(E', E, T)/dE'$. Window function scales contributions of energy states in transport measurements near given energy E.[38] Besides the temperature also complex absorbing potential gives rise to broadening of DOS as it introduces disorder at the edge of TBLG.[36]

III. RESULTS AND DISCUSSION

Results presented in this section were obtained for local biasing TBLG within a circle area of radius $R_c = 80\,nm$ with edge smoothed by factor $\sigma_c = 5\,nm$ which is constant for three considered twist angles $\theta = 0.75^0$, 1.05^0 and 2^0. These give set of Moire lattice constants $L_m = 18.8$, 13.4, and 7.05 nm.

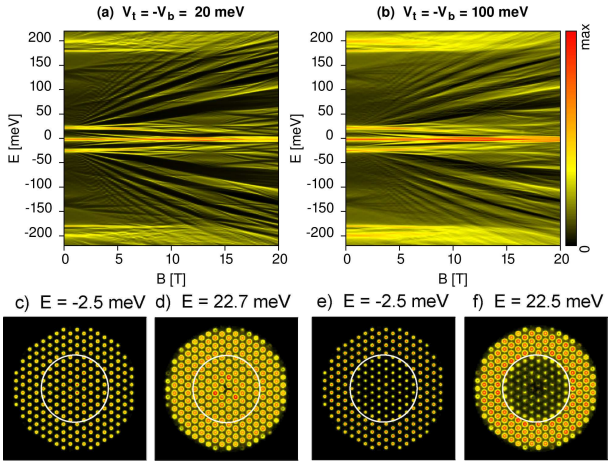

FIG. 1: (Color online) DOS (upper row) and LDOS (lower row) for TBLG with central biased region, parameters used in calculations: $\theta = 0.75^0$, $V_t = -V_b = 20$ meV (a,c,d) and $V_t = -V_b = 100$ meV (b,e,f). In (c)-(f) obtained for $B = 1$ T energies are displayed on top while the thick white circle marks approximately an edge of cavity ($R_c = 80$ nm).

DOS calculated for $\theta = 0.75^0$ is shown in Fig.1. Even though top and bottom layers in central part are biased asymmetrically [Fig.1(a)], the particle-hole symmetry is slightly broken due to interlayer coupling w_{AA}.[16] For this reason the charge neutrality point (CNP) localizes at $E \approx -2$ meV where two van Hove singularity peaks merge.[11,14,15,39] Irrespective of magnetic field variations CNP does not change its energy and forms zero-mode Landau level (ZMLL).[40] It is flanked by two satellites shifted by ± 24 meV which positions are robust against changes of amplitude of polarization potential [cf. Figs.1(a) and (b)] but are splitted for magnetic field $B > 5\,T$. Note however that ZMLL splits for[41] $B > B_c \approx 3.3\,\theta^2 = 1.9$ T as for generic TBLG. At moderate magnetic field strength, the magnetic effects dominate the kinetic energy of Dirac particles and Landau levels becomes easily recognizable due to their characteristic B dependence $E_n = E_{CNP} + sgn(n)\sqrt{2e\hbar v_f^2 |n| B}$ for integer n. Due to relatively large Moire lattice constant ($L_m = 18.8$ nm) the magnetic flux piercing Moire unit cell ϕ_m and quantum of magnetic flux ϕ_0 are comparable. For such conditions, by virtue of Hofstadter theory,[28] each single energy band must split what manifests in self-similarity of resultant energy spectrum. Despite occurrence of distinct wide LLs fans in Figs.1(a) and 1(b) for $\theta = 0.75^0$, formation of fractal pattern in energy spectra (Moire butterflies[5,29]) is hardly recognizable. This feature becomes apparent for lager twist angle considered here, namely $\theta = 1.05^0$, what we notice in Fig.2(a) around $B = 14$T. Direct comparison of four cases presented in this figure reveals that low opposite biasing of layers is preferable to other conditions [cf. Fig.2(a) and Figs.2(b)-(d)] which largely suppress this subtle effect.

LDOS calculated for $\theta = 0.75^0$ and $B = 1$ T presented in Figs.1(c)-(d) for two VHS peaks shows that for low opposite bias ($V_t = -V_b = 20$ meV) it is composed of AA centered spatially-separated point-like as well as small ring-like density grains which spreads over generic TBLG and biased region. That partly results from applying potential difference to layers since it opens a gap in Bernal stacking AB/BA sites.[42] Then at contacts of these regions, on a line connecting closest AA sites, one-dimensional transport channels are formed which are topologically protected for small twist angles($\theta < 0.5^0$).[6,17,43–45]

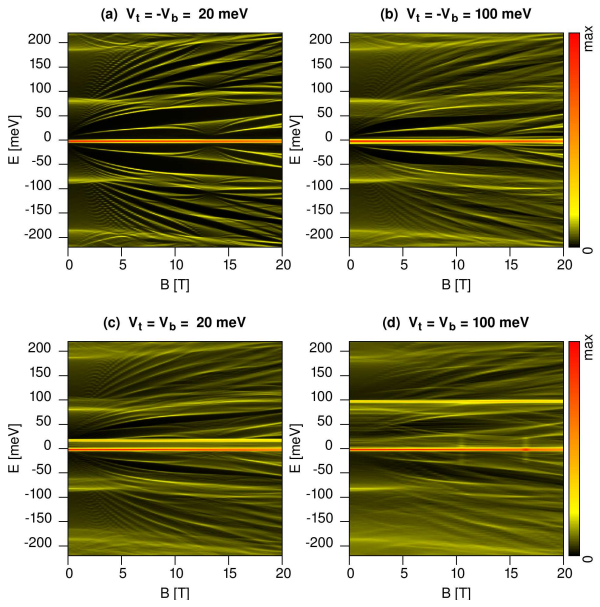

FIG. 2: (Color online) TBLG energy spectra for $\theta = 1.05^0$ with counter-polarization of layers $V_t = -V_b$ (first row) and the same polarization $V_t = V_b$ (second row) of layers in central region.

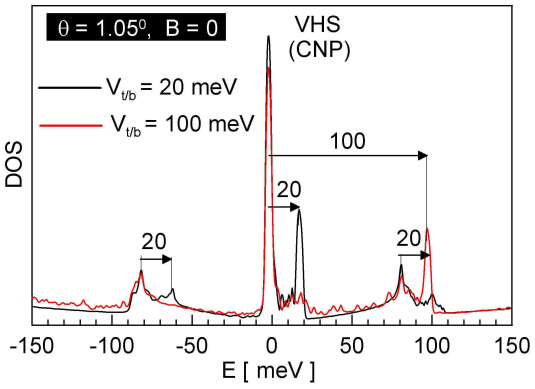

FIG. 3: (Color online) DOS for TBLG with twist $\theta = 1.05^0$, $B = 0$, and two cavity's potentials $V_{t/b} = 20$ meV (black) and $V_{t/b} = 100$ meV (red). Arrows with numbers show direction and approximate shift of dubbed states.

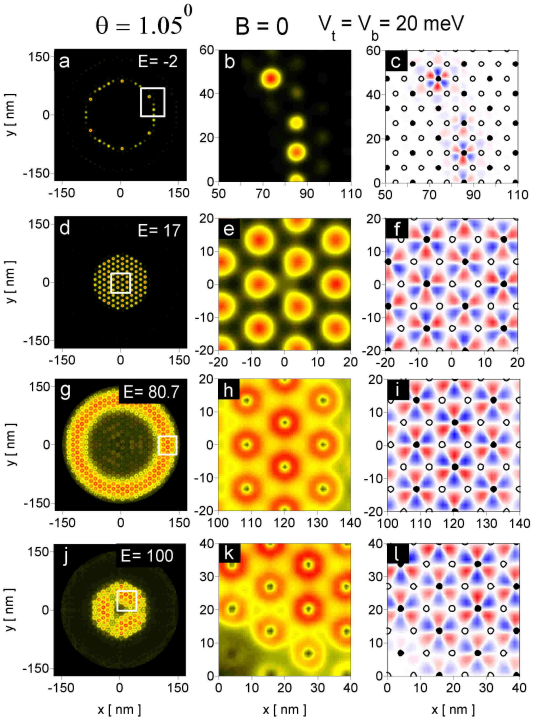

FIG. 4: (Color online) LDOS (first and second columns) and vorticity of current (third column) for $\theta = 1.05^0$, bias potential $V_t = V_b = 20$ meV and $B = 0$. Energies displayed in first column correspond to DOS peaks presented in Fig.3 (black). Full (empty) dots in vorticity maps show positions of AA (AB/BA) sites.

As already mentioned DOS for first magic angle ($\theta = 1.05^0$) displayed in Figs.2(a) and (b) show more distinct manifestation of fractal structure of LLs which are shifted towards slightly stronger magnetic fields. Position of ZMLL do not change but VHS satellites move away by $\Delta E_1 \approx \pm 81$ meV and again their positions are independent of amplitude of applied bias provided that layers in center of TBLG are counter-polarized [cf. Figs.2(a) and (b)]. That picture will change if both layers are identically polarized what show Figs. 2(c) and 2(d). Since biasing of graphene layers in central region is the same the energy structure captured within it is pushed up by about $\Delta E \approx V_{t/b}$. The most striking evidence of doubling the number of energy levels is occurrence of second ZMLL which stays insensitive to magnetic field. Moreover in Fig.2(c) we see that both DOS satellites are also replicated as there occur two, but less intensive, DOS peaks shifted upwards by about 20 meV. For stronger central biasing ($V_t = V_b = 100$ meV) this shift could be hardly resolved, besides strong look-alike ZMLL, but undeniably must exist since crossings of LLs are visible even in moderate magnetic field $B = 5 - 10$ T [see Fig.2(d)].

Doubling of energy structure for identical biasing of layers becomes most distinct for vanishing magnetic field. Figure 3 shows two DOS spectra for $B = 0$ which do not change much for $B < 5$ T. We see that central (CNP)

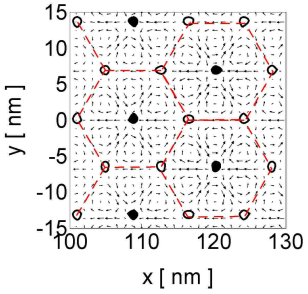

FIG. 5: (Color online) Vector plot of current for the same parameters as in Fig.4(g) ($E = 80.7$ meV).

and flanking VHS peaks are duplicated and their copies, few times smaller, are shifted upwards in energy in accordance with bias potential applied to both layers $V_t = V_b$. LDOS maps displayed in Fig.4 show that CNP and its neighbouring VHS are pushed outside cavity (first and third row) what explains their insensitivity to variations of bias potential. That differ them from their shifted counterparts, which as expected, are largely localized in cavity [see Figs.4(d) and (j)]. Although cavity has finite extensions, for $R_c = 80$ nm and $L_m = 13.4$ nm it covers $n_m \approx 4\pi R_c^2/(\sqrt{3}l_m^2) \approx 257$ Moire supercells, enough to develop additional energy quasi-bands separated from the ones formed for unbounded and unbiased rest part of TBLG. Even though, the renormalized Fermi velocity is considerably suppressed in vicinity of each magic angle[9] enhancing thus particle localization around AA sites for low energy [see Figs.4(a),(b), (d) and (e)], the tunneling on Moire lattice between AA sites is supported by helical current. An example of current density is shown in Fig.5 which in considered cases is hardly readable, instead we will show vorticity of current $v_j = (\nabla \times \vec{j})_z$ which nodal surface separates countercirculating currents. Pattern of current vorticity [last column in Fig.4], similar for all AA sites with respect to local variations in intensity, is composed of triangle-shaped three current vortices and three antivortices connected at AA sites. Due to bending of particle's trajectory within each current vortex only its edge part can couple to neighbouring counter-oriented vortex, at midway between AA sites, by bending the wave vector drawing thus simple or reflected elongated S-like path. Surprisingly, even though density rings centered at AA sites are weakly connected with straight bridges [Figs.4(e) and (h)], the pattern of current vorticity does not change. This specific orbital antiferromagnetic property of Moire supercells is valid only if interactions are weak, otherwise, as shown in Ref.[46], applying large interlayer bias potential may trigger transition from the lattice antiferromagnetic phase to the spiral ferromagnetic one in TBLG. Interactions can also enhance spin and valley polarizations triggered by variations of symmetry breaking small magnetic field giving rise to anomalous Hall effect.[25,26] Since in considered system the interlayer biasing is local we expect that such geometry would, under properly chosen conditions, allow to create and control different magnetic phases in adjacent spatial regions.

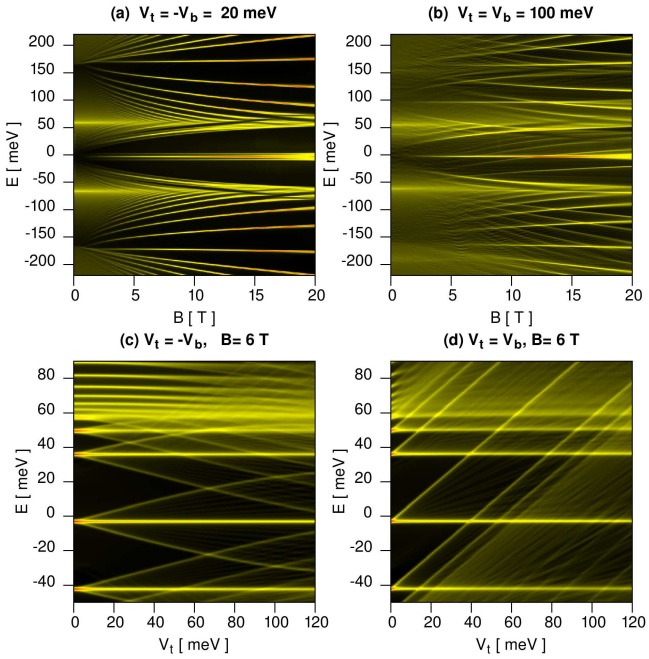

FIG. 6: (Color online) DOS for $\theta = 2^0$, $R_c = 80$ nm in function of B for $V_t = -V_b = 20$ meV (a) and the same polarization of layers $V_t = V_b = 100$ meV (b), figures (c) and (d) show LLs' satellites for counter- and the same polarization of layers at $B = 6$ T.

Increasing further the twist angle to $\theta = 2^0$ substantially changes the DOS evolution in magnetic field. Figure 6 shows that states will start to condense on LLs even for small magnetic field ($B > 2\,T$) and moderate energies ($E \approx 150$ meV). Moreover, due to shifting van Hove's singularities to $E = -66$ and 59 meV ($\Delta E_{VHS} = 125$ meV) DOS at CNP is minimal but zero mode LL is restored for higher B. Positions of VHS peaks in generic TBLG can be approximated[39] as $\Delta E_{VHS} = \hbar V_F \Delta K - 2t^\theta$ which for $\theta = 2^0$, $t^\theta \approx 0.4\, t_\perp$ and $t_\perp = 3\, w_{AA}$ gives 127 meV. Although LDOS for maxima of VHS go outside the cavity, similarly as for $\theta = 1.05^0$, there was achieved satisfactory agreement. It is worth to note however that value of $t_\perp$ we used is noticeably larger from originally proposed ones[39] ($t_\perp =$ 240 and 270 meV), on the other hand the dependence of VHS positions on twist angle generally varies for different substrate the TBLG is put on.[47,48]

We have checked that small interlayer bias ($V_t = V_b =$ 20 meV) as shown in Fig.6(a) gives almost similar pattern as for unbiased case besides the small satellite peaks flanking lowest LL's. These satellites are sensitive to the variations of bias potential what we notice in Fig.6(c). Each pair of satellites originates from single LL state and increasing bias potential shifts positions of flanking states towards higher or lower energy as if most parts of these states are accumulated at upper or at lower layer. They

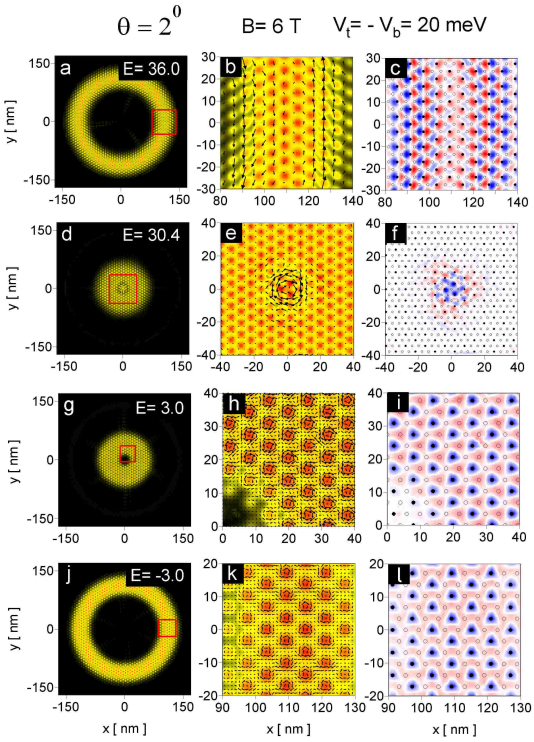

FIG. 7: (Color online) LDOS (left column), its enlarged part (red rectangle) with vector plot of current (middle column) and vorticity of current (right column) for zero mode LL (lowest row) and next LL (top row) and their satellites (middle rows) calculated for $V_t = -V_b = 20$ meV and $B = 6$ T. Full (empty) dots in maps of current vorticity show positions of AA (AB/BA) sites.

may cross with other ones originating from neighbouring LLs. Additionally, we see in Fig.6(c) that the lowest LLs are insensitive to bias potential even though it extends over a large area in center of TBLG. Such unusual behaviour we explain by analyzing LDOS for ZMLL, first LL and their two satellites which are shown in Fig.7 for $B = 6$ T. LDOS for ZMLL ($E = -3$ meV) as well as for first LL ($E = 36$ meV) is pushed outside the cavity and due to magnetic deflection both form a ring-like structure. The enlarge parts of LDOS (second column) show however, that ZMLL density islands are localized at AA sites with largely disconnected current loops circulating around each AA site. Although, all sites AA gives nonzero net magnetization for ZMLL what we deduce from the current vorticity, these are surrounded by AB and BA regions with opposite vorticity leading eventually to their cancellation. For 1LL [Figs.7(b) and (c)] maxima of LDOS at AA sites becomes less distinct, here however current loops from neighbouring AA sites merge and consequently the density current flows in clockwise (counterclockwise) direction on inner (outer) side of ring-like LDOS. Current flowing through AA and AB/BA sites is only slightly locally deflected but its global orientation remains unchanged. Second and third rows in Fig.7 shows results for LLs' satellites. Both are largely localized inside of central region and therefore they must be sensitive to interlayer bias potential. Despite stronger accumulation of these states at upper or lower layer, their properties are still remarkably influenced by interlayer coupling. The one which decouples from ZMLL (third row) has distinct AA island-like LDOS structure with current loops circulating around similarly as for ZMLL. Second satellite (second row) besides clear triangle pattern in LDOS develops current vortex in the very center of TBLG while the current almost vanishes outside.

Contrary to this case, by applying the same potential to both layers [see Fig.6 (b)] makes DOS spectra more complicated even for large magnetic field where LLs cross each other. In this case each LL has only one satellite shifted towards higher energy due to identical polarization of layers [see Fig.6(d)]. These, however, are less pronounced than LLs and can not form such distinctive crossings as we see in Fig.6(b). Because spatial size of considered cavity is large ($R_c = 80$ nm) as compared to present Moire lattice constant ($L_m = 7.05$ nm) that gives enough space to develop look-alike LLs structure shifted upwards by $V_t = V_b = 100$ meV. We have confirmed this by conducting additional calculations for $V_t = V_b$ but limiting the biased region to $R = 50$ nm (results not show here). The outcomes showed only generic TBLG DOS states merging into LLs as in Fig.6(a) because central biased region has not enough space to develop its own energy pseudobands. The look-alike energy states we already observed for $\theta = 1.05^0$ in Figs.2 (c) and (d), where second ZMLL state has emerged for $E = 20$ and 100 meV accordingly with bias potential. However, due to much attenuated DOS spectra in those cases we can not definitely claim if the whole low-energy spectra was duplicated or only its part. Certainly, very recognizable peaks localized near $E \sim \pm 81$ meV [see Fig. 3] have counterparts shifted upward in energy by $V_t = V_b = 20$ meV. Other look-alike states, if even exist for larger B, are hardly recognizable due to strongly broaden spectra.

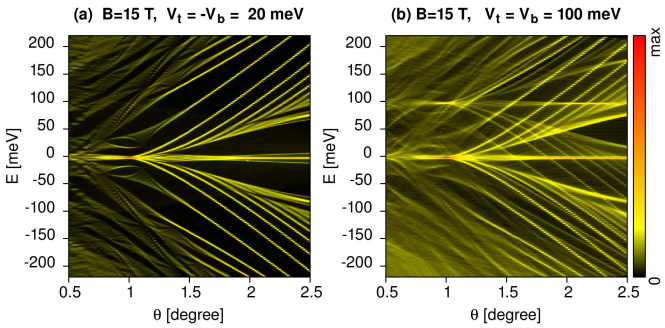

FIG. 8: (Color online) Energy spectra of TBLG for parameters $R_c = 80$ nm, $B = 15$ T, $V_t = -V_b = 20$ meV (a) and $V_t = V_b = 100$ meV (b) in function of the twist angle.

Results presented so far indicate that twist angle plays crucial role in doubling the number of LL states. To confirm this we will analyze DOS in function of twist an-

gle, results for identical and counter-biasing of layers in strong magnetic field ($B = 15\,T$) are presented in Fig.8. Interestingly, in counter-biasing case [Fig.8(a)] the low energy spectrum develops fractal pattern for $\theta \leq 1.05^0$ as well as for larger energies until $\theta < 1.5^0$. Increasing twist angle beyond first magic angle separates the ZMLL from other LLs. Due to both, counter-biasing and strong magnetic field, the flanking satellite states are hardly visible besides the ZMLL for $\theta > 2^0$. However, by applying the same bias potential to layers substantially changes energy spectra. For $V_t = V_b = 100$ meV we easily recognize in Fig.8(b) look-alike second LLs branch. These states are shifted upwards and surprisingly reconstruct also the self-similarity feature of energy spectra for $\theta < 1.05^0$.

IV. CONCLUSIONS

We used continuum model to study the Landau levels formed in twisted bilayer graphene with bias potential applied in its center. Although the electrons can not be confined definitely in space due to gapless energy structure of generic TBLG, the combined effect of magnetic and electrostatic deflection applied on their trajectories can enhance their momentary spatial localization and thus largely enrich resultant energy spectrum. Namely, we observe formation of distinct Landau levels with characteristic fractal pattern arising in moderate magnetic field ($B < 20$T) for small twist angle $\theta < 2^0$ provided that layers in central region are counter-biased. In this case, the lowest LLs are localized outside cavity forming a ring-like structure. When the same bias is applied to both layer, the energy spectrum becomes messy as it contains two branches of LLs crossing each other. The second branch is shifted in energy according to applied bias and is developed by states strongly localized within spatially limited biased region. These look-alike energy states can be formed provided that the ratio of biased region size and Moire lattice constant is large enough which we estimate to be at least $R_c/L_m > 5 \div 7$. For identical and counter-biasing of layers each Landau level becomes a precursor of one (electron-like or hole-like) and two (electron-like and hole-like) flanking states, respectively. Energies of these satellites change approximately linearly with bias potential since they are largely localized in center of TBLG system. Since density of states in TBLG can be sampled in STM experiments locally giving the same pattern irrespective of spatial position over TBLG plane,[30] we think the existence of described here look-alike states as well as flanking states could be verified at least for case with identical biasing of layers in TBLG nanodevice with split back gate. This would be possible for $\theta \sim 2^0$ while for smaller twist angles $\theta \approx 1.1^0$, as show STM experiments,[49] occurrence of spatial distortions in Moire lattice when energy of tunneling electrons is tuned to VHS positions may suppress considered effects.

Acknowledgements

This work was (partially) supported by the AGH UST statutory tasks No. 11.11.220.01/2 within subsidy of the Ministry of Science and Higher Education.

References

* Electronic address: chwiej@fis.agh.edu.pl

[1] K. S. Novoselov, A. Mishchenko, A. Carvalho, and A. H. Castro Neto, **353** (2016).
[2] S.-Y. Li, Y. Zhang, Y.-N. Ren, J. Liu, X. Dai, and L. He, Phys. Rev. B **102**, 121406 (2020).
[3] H. Overweg, H. Eggimann, X. Chen, S. Slizovskiy, M. Eich, R. Pisoni, Y. Lee, P. Rickhaus, K. Watanabe, T. Taniguchi, et al., Nano Letters **18**, 553 (2018).
[4] H. Yoo, R. Engelke, S. Carr, S. Fang, K. Zhang, P. Cazeaux, S. H. Sung, R. Hovden, A. W. Tsen, T. Taniguchi, et al., Nature Materials **18**, 448 (2019).
[5] K. Kim, A. DaSilva, S. Huang, B. Fallahazad, S. Larentis, T. Taniguchi, K. Watanabe, B. LeRoy, A. H. MacDonald, and E. Tutuc, Proceedings of the National Academy of Sciences **114**, 3364 (2017).
[6] S. Huang, K. Kim, D. K. Efimkin, T. Lovorn, T. Taniguchi, K. Watanabe, A. H. MacDonald, E. Tutuc, and B. J. LeRoy, Phys. Rev. Lett. **121**, 037702 (2018).
[7] E. J. Mele, Phys. Rev. B **81**, 161405 (2010).
[8] E. J. Mele, Phys. Rev. B **84**, 235439 (2011).
[9] R. Bistritzer and A. H. MacDonald, Proceedings of the National Academy of Sciences **108**, 12233 (2011).
[10] J. M. B. Lopes dos Santos, N. M. R. Peres, and A. H. Castro Neto, Phys. Rev. Lett. **99**, 256802 (2007).
[11] J. M. B. Lopes dos Santos, N. M. R. Peres, and A. H. Castro Neto, Phys. Rev. B **86**, 155449 (2012).
[12] W.-X. Wang, H. Jiang, Y. Zhang, S.-Y. Li, H. Liu, X. Li, X. Wu, and L. He, Phys. Rev. B **96**, 115434 (2017).
[13] W. Yan, M. Liu, R.-F. Dou, L. Meng, L. Feng, Z.-D. Chu, Y. Zhang, Z. Liu, J.-C. Nie, and L. He, Phys. Rev. Lett. **109**, 126801 (2012).
[14] I. Brihuega, P. Mallet, H. González-Herrero, G. Trambly de Laissardière, M. M. Ugeda, L. Magaud, J. M. Gómez-Rodríguez, F. Ynduráin, and J.-Y. Veuillen, Phys. Rev. Lett. **109**, 196802 (2012).
[15] G. Trambly de Laissardiere, D. Mayou, and L. Magaud, Nano Letters **10**, 804 (2010).
[16] G. Tarnopolsky, A. J. Kruchkov, and A. Vishwanath, Phys. Rev. Lett. **122**, 106405 (2019).
[17] P. Rickhaus, J. Wallbank, S. Slizovskiy, R. Pisoni, H. Overweg, Y. Lee, M. Eich, M.-H. Liu, K. Watanabe, T. Taniguchi, et al., Nano Letters **18**, 6725 (2018).
[18] H. Shi, Z. Zhan, Z. Qi, K. Huang, E. v. Veen, J. A. Silva-Guillén, R. Zhang, P. Li, K. Xie, H. Ji, et al., Nature Communications **11**, 371 (2020).
[19] Y. Cao, V. Fatemi, S. Fang, K. Watanabe, T. Taniguchi,

E. Kaxiras, and P. Jarillo-Herrero, Nature **556**, 43 (2018).
[20] M. Yankowitz, S. Chen, H. Polshyn, Y. Zhang, K. Watanabe, T. Taniguchi, D. Graf, A. F. Young, and C. R. Dean, **363**, 1059 (2019).
[21] Y. Cao, V. Fatemi, A. Demir, S. Fang, S. L. Tomarken, J. Y. Luo, J. D. Sanchez-Yamagishi, K. Watanabe, T. Taniguchi, E. Kaxiras, et al., Nature **556**, 80 (2018).
[22] A. Kerelsky, L. J. McGilly, D. M. Kennes, L. Xian, M. Yankowitz, S. Chen, K. Watanabe, T. Taniguchi, J. Hone, C. Dean, et al., Nature **572**, 95 (2019).
[23] A. L. Sharpe, E. J. Fox, A. W. Barnard, J. Finney, K. Watanabe, T. Taniguchi, M. A. Kastner, and D. Goldhaber-Gordon, **365**, 605 (2019).
[24] X. Lu, P. Stepanov, W. Yang, M. Xie, M. A. Aamir, I. Das, C. Urgell, K. Watanabe, T. Taniguchi, G. Zhang, et al., Nature **574**, 653 (2019).
[25] M. Serlin, C. L. Tschirhart, H. Polshyn, Y. Zhang, J. Zhu, K. Watanabe, T. Taniguchi, L. Balents, and A. F. Young, **367**, 900 (2020).
[26] A. L. Sharpe, E. J. Fox, A. W. Barnard, J. Finney, K. Watanabe, T. Taniguchi, M. A. Kastner, and D. Goldhaber-Gordon, **365**, 605 (2019).
[27] S. Carr, D. Massatt, S. Fang, P. Cazeaux, M. Luskin, and E. Kaxiras, Phys. Rev. B **95**, 075420 (2017).
[28] D. R. Hofstadter, Phys. Rev. B **14**, 2239 (1976).
[29] R. Bistritzer and A. H. MacDonald, Phys. Rev. B **84**, 035440 (2011).
[30] Z. F. Wang, F. Liu, and M. Y. Chou, Nano Letters **12**, 3833 (2012).
[31] C. R. Dean, L. Wang, P. Maher, C. Forsythe, F. Ghahari, Y. Gao, J. Katoch, M. Ishigami, P. Moon, M. Koshino, et al., Nature **497**, 598 (2013).
[32] W.-Y. He, Z.-D. Chu, and L. He, Phys. Rev. Lett. **111**, 066803 (2013).
[33] K. Varga and J. A. Driscoll, *Computational Nanoscience: Applications for Molecules, Clusters, and Solids* (Cambridge University Press, 2011).
[34] B. Feldman, T. Seideman, O. Hod, and L. Kronik, Phys. Rev. B **90**, 035445 (2014).
[35] G. Calogero, N. R. Papior, P. Bøggild, and M. Brandbyge, Journal of Physics: Condensed Matter **30**, 364001 (2018).
[36] M. Andelković, L. Covaci, and F. M. Peeters, Phys. Rev. Materials **2**, 034004 (2018).
[37] K. Uchida, S. Furuya, J.-I. Iwata, and A. Oshiyama, Phys. Rev. B **90**, 155451 (2014).
[38] S. Datta, *Electronic Transport in Mesoscopic Systems* (Cambridge University Press, 1995).
[39] G. Li, A. Luican, J. M. B. Lopes dos Santos, A. H. Castro Neto, A. Reina, J. Kong, and E. Y. Andrei, Nature Physics **6**, 109 (2010).
[40] R. de Gail, M. O. Goerbig, F. Guinea, G. Montambaux, and A. H. Castro Neto, Phys. Rev. B **84**, 045436 (2011).
[41] P. Moon and M. Koshino, Phys. Rev. B **85**, 195458 (2012).
[42] E. V. Castro, K. S. Novoselov, S. V. Morozov, N. M. R. Peres, J. M. B. L. dos Santos, J. Nilsson, F. Guinea, A. K. Geim, and A. H. C. Neto, Phys. Rev. Lett. **99**, 216802 (2007).
[43] P. San-Jose and E. Prada, Phys. Rev. B **88**, 121408 (2013).
[44] D. K. Efimkin and A. H. MacDonald, Phys. Rev. B **98**, 035404 (2018).
[45] B. Tsim, N. N. T. Nam, and M. Koshino, Phys. Rev. B **101**, 125409 (2020).
[46] L. A. Gonzalez-Arraga, J. L. Lado, F. Guinea, and P. San-Jose, Phys. Rev. Lett. **119**, 107201 (2017).
[47] L.-J. Yin, J.-B. Qiao, W.-X. Wang, W.-J. Zuo, W. Yan, R. Xu, R.-F. Dou, J.-C. Nie, and L. He, Phys. Rev. B **92**, 201408 (2015).
[48] A. Luican, G. Li, A. Reina, J. Kong, R. R. Nair, K. S. Novoselov, A. K. Geim, and E. Y. Andrei, Phys. Rev. Lett. **106**, 126802 (2011).
[49] S.-Y. Li, K.-Q. Liu, L.-J. Yin, W.-X. Wang, W. Yan, X.-Q. Yang, J.-K. Yang, H. Liu, H. Jiang, and L. He, Phys. Rev. B **96**, 155416 (2017).